MHD TURBULENCE AND MAGNETIC DYNAMOS

SHEBALIN JOHN V.
Astromaterials Research Office/NASA Johnson Space Center, Houston, TX 77058, USA
E-mail: john.v.shebalin@nasa.gov

Abstract : An inherent dynamo process exists in magnetohydrodynamic turbulence and is statistical in nature. Turbulent planetary and stellar magnetofluids exhibit large-scale magnetic fields and this statistical process may be involved in the origin of these fields.

1. Introduction

Turbulent magnetohydrodynamic (MHD) flows are expected to exist inside astrophysical [1] and geophysical [2] objects, and have also been seen in laboratory dynamo experiments [3]. In these physical systems, coherent large-scale magnetic fields are observed and appear to arise from an internal dynamo process. In turn, numerical experiments have shown that coherent, large-scale magnetic fields arise spontaneously in incompressible, homogeneous MHD turbulence, an effect that is especially clear in the ideal case, when viscosity and resistivity are zero [4,5], but is also evident in the dissipative case [6]. The inherent dynamo in MHD turbulence is statistical and involves broken ergodicity manifesting itself as a broken symmetry. The theory of this inherent dynamo has been elucidated relatively recently [7,8] and the aim here is to give a qualitative overview of the connection between MHD turbulence and magnetic dynamos; further mathematical details can be found in the references cited.

2. Ideal MHD turbulence

The Earth, due to its proximity, is our best-studied planetary body with regard to MHD dynamos and much has been written about it, e.g., [9]. The essential facts are that the Earth has a solid inner core and a large fluid outer core, both composed mostly of iron, as well as a mantle and then a crust overlying the core. Although density varies from top to bottom in the outer core by about 20 percent, the magnetofluid is usually treated as incompressible, allowing for a simplified mathematical model of its MHD flows. In addition, it is expected that kinetic and magnetic Reynolds numbers are large enough, and that there is enough convective stirring occurring, so that the outer core is filled with turbulent magnetofluid. In taking the limit of infinitely large Reynolds numbers, we arrive at ideal, incompressible MHD turbulence. The primary dynamical variables are the turbulent velocity field $\mathbf{u}$ and the turbulent magnetic field $\mathbf{b}$; these are functions of time and position and satisfy $\nabla\cdot\mathbf{u} = \nabla\cdot\mathbf{b} = 0$. The basic equations of incompressible MHD turbulence are well known and are discussed in detail elsewhere, e.g., [10]. (Here we discuss only three-dimensional MHD turbulence.)

To theoretically study and numerically simulate MHD turbulence, we use so-called Galerkin expansions, summations over a complete set of orthogonal basis functions, each with its own coefficient, to represent either $\mathbf{u}$ or $\mathbf{b}$. Each term in the series satisfies given boundary conditions (b.c.s) and any other requirements that are imposed, so that a truncated expansion can approximate $\mathbf{u}$ or $\mathbf{b}$ to the desired accuracy. For example, if periodic b.c.s are used, then a Fourier (trigonometric) series is appropriate, while for a spherical shell with homogeneous b.c.s (to be defined below), then expansion in terms of spherical Bessel function-spherical harmonics can be employed. Galerkin basis functions are smooth and continuous, so that exact spatial partial derivatives can be found, while time dependence is completely contained in the expansion coefficients. In essence, a Galerkin method transforms the partial differential MHD equations into a finite set of nonlinear, coupled, ordinary differential equations.

The simplest geometry for analysis and simulation of a confined magnetofluid is that of a box with periodic b.c.s. The spherical case is more pertinent for the geodynamo, but b.c.s suitable for theory and computation must be determined. First, we assume that the outer core has concentric, spherical boundaries. The confined magnetofluid is ideal and the magnetic field is said to be 'locked into the flow field,' which moves it about, stretching and bending it. The magnetic field reacts back on the flow field and attempts to move it around, in turn. In this case, we assume that near solid physical boundaries, except in a thin boundary layer, both velocity and magnetic fields are essentially parallel to the boundary and that only inside the boundary layer does the magnetic field grow a nonzero component normal to the solid boundary. Then, for our mathematical boundaries, we use virtual spherical surfaces, sitting on top of the boundary layers, where we impose 'homogeneous b.c.s.' These homogeneous b.c.s are such that all primary (velocity and magnetic) fields and all derived fields (vorticity, electric current, magnetic vector potential) have zero normal components, but unconstrained parallel components, on the homogeneous boundaries [11]. (Homogeneous b.c.s appear justified when we look at numerical solutions from non-ideal MHD simulations with non-homogeneous b.c.s [12].) It turns out that the statistical mechanics of ideal MHD turbulence takes essentially the same form in either a periodic box [8] or in a spherical shell with homogeneous b.c.s [11], so that Fourier analysis and simulation serve as a viable surrogate for the seemingly more realistic spherical Bessel function-spherical harmonic approach.

3. Statistical mechanics

The set of expansion coefficients representing ideal MHD turbulence forms a conservative dynamical system that generally has not just one, but three constants of the motion: the energy $E = \frac{1}{2}\int(u^2+b^2)dV$, cross helicity $H_C = \frac{1}{2}\int\mathbf{u}\cdot\mathbf{b}dV$ and magnetic helicity $H_M = \frac{1}{2}\int\mathbf{a}\cdot\mathbf{b}dV$; the magnetic vector potential $\mathbf{a}$ is defined by $\nabla\times\mathbf{a} = \mathbf{b}$ and $\nabla\cdot\mathbf{a} = 0$, and integration is over the bounded volume V. When V rotates as a whole, H_C is no longer constant, but $\rightarrow 0$ with time. Let $\tilde{\mathbf{u}}(\mathbf{k},t)$ and $\tilde{\mathbf{b}}(\mathbf{k},t)$ represent expansion coefficients for the velocity and magnetic field, respectively. The wave vectors $\mathbf{k}$ have components such that $|\mathbf{k}| \le K < \infty$; the lowest values of $k = |\mathbf{k}|$ correspond to the longest length-scale in the physical volume. The set of all independent velocity and magnetic field coefficients defines the phase space Γ of the dynamical system, whose dimension is proportional to K^3. Statistically, the system is described by a canonical ensemble with partition function $Z = \int\exp(-\alpha E - \beta H_C - \gamma H_M)d\Gamma$; integration is over all of phase space Γ and the cofactors α, β and γ are called 'inverse temperatures' or 'undetermined multipliers' as their values are initially unknown. The probability density function is given by $D = Z^{-1}\exp(-\alpha E - \beta H_C - \gamma H_M)$ and may be used to determine expectation values for the two independent, complex components of $\tilde{\mathbf{u}}(\mathbf{k})$ or $\tilde{\mathbf{b}}(\mathbf{k})$.

Historical and theoretical details of ideal MHD statistics may be found elsewhere [8]. Here, only those details needed for a brief, qualitative discussion will be mentioned. To begin, the three inverse temperatures α, β and γ may be expressed as functions of only one unknown variable φ, which we have chosen to be the expectation value of the magnetic energy. Thus, the entropy functional of the system, $\sigma(\varphi) = -\int D\log D\,d\Gamma$ is also a function of φ. As is well known [13], entropy is the minimum of the entropy functional. The value of φ appropriate for the finite dynamical system with given E, H_C and H_M is then found by determining the value $\varphi = \varphi_o$ that minimizes $\sigma(\varphi)$. Requiring $d\sigma(\varphi)/d\varphi = 0$ yields $2\varphi_o \approx E + \kappa|H_M|[1 - (H_C/\varphi_o)^2]$, after much work [8,11], where and $\kappa|H_M| < E$, and where $\kappa = 1$ for the periodic box Fourier case [8], while $\kappa \approx 1.8638$ for a spherical shell geodynamo [11]. When the volume V is

rotating as a whole, $H_C \to 0$ and $\varphi_o \approx \frac{1}{2}(E + \kappa|H_M|)$. In addition, analysis reveals that the energy in the longest wavelength mode is O(N) times greater than in any shorter wavelength mode in the system, where N is the number of modes (i.e., independent values of **k** in the Galerkin expansion). This is in contradistinction to ideal fluid turbulence, where the smallest length-scale modes have the most energy [14]. Dissipation depletes smallest length-scale modes quickly of their energy, while leaving the largest-scale modes relatively untouched. Thus, ideal results have much less relevance to real fluid turbulence, which has a direct cascade to smaller length scales in its energy spectrum [14], than for real MHD turbulence, which has an inverse cascade to larger length scales [15].

An advance in the statistical mechanics of ideal MHD turbulence was the discovery of ideal eigenmodes [7]. The phase space probability density D is a product of modal densities of the form $D_{\mathbf{k}} \sim \exp[-\tilde{\mathsf{y}}^\dagger(\mathbf{k})\,\mathsf{M}_k\,\tilde{\mathsf{y}}(\mathbf{k})]$; $\tilde{\mathsf{y}}$ is a 4 component, complex column vector whose Hermitean adjoint is $\tilde{\mathsf{y}}^\dagger = [\tilde{u}_1^*(\mathbf{k})\ \tilde{u}_2^*(\mathbf{k})\ \tilde{b}_1^*(\mathbf{k})\ \tilde{b}_2^*(\mathbf{k})]$; here, '*' denotes complex conjugate, $\tilde{u}_i(\mathbf{k})$ and $\tilde{b}_i(\mathbf{k})$, i = 1, 2, are the independent components of $\tilde{\mathbf{u}}(\mathbf{k})$ and $\tilde{\mathbf{b}}(\mathbf{k})$, and M_k is the modal Hermitean covariance matrix. We solve the matrix equation $\mathsf{M}_k\tilde{\mathsf{e}} = \lambda\tilde{\mathsf{e}}$ to find eigenvalues λ and eigenvectors $\tilde{\mathsf{e}}$; the matrix M_k, and its eigenvalues $\lambda_k^{(i)}$, i = 1,2,3,4, are

$$\mathsf{M}_k = \begin{bmatrix} \alpha & 0 & \beta/2 & 0 \\ 0 & \alpha & 0 & \beta/2 \\ \beta/2 & 0 & \alpha & -i\gamma/k \\ 0 & \beta/2 & i\gamma/k & \alpha \end{bmatrix}, \quad \begin{aligned} \lambda_k^{(1)} &= \alpha - \tfrac{1}{2}(\eta_k + \gamma/k) \\ \lambda_k^{(2)} &= \alpha + \tfrac{1}{2}(\eta_k + \gamma/k) \\ \lambda_k^{(3)} &= \alpha + \tfrac{1}{2}(\eta_k - \gamma/k) \\ \lambda_k^{(4)} &= \alpha - \tfrac{1}{2}(\eta_k - \gamma/k) \end{aligned}, \quad \eta_k = \sqrt{\beta^2 + \frac{\gamma^2}{k^2}}. \tag{1}$$

The explicit form of eigenvectors $\tilde{\mathsf{e}}_i(\mathbf{k})$ and transformation matrix U_k are given elsewhere [8]. Corresponding to the eigenvalues $\lambda_k^{(i)}$, i = 1,2,3,4, the transformed vector $\tilde{\mathsf{v}}(\mathbf{k}) = \mathsf{U}_k^\dagger\tilde{\mathsf{y}}(\mathbf{k})$ has components $\tilde{v}_i(\mathbf{k})$:

$$\begin{aligned} \tilde{v}_1(\mathbf{k}) &= \overline{\beta}\zeta_k^-\left[\tilde{u}_1(\mathbf{k}) + i\tilde{u}_2(\mathbf{k})\right] - \zeta_k^+\left[\tilde{b}_1(\mathbf{k}) + i\tilde{b}_2(\mathbf{k})\right] \\ \tilde{v}_2(\mathbf{k}) &= \overline{\beta}\zeta_k^-\left[\tilde{u}_1(\mathbf{k}) - i\tilde{u}_2(\mathbf{k})\right] + \zeta_k^+\left[\tilde{b}_1(\mathbf{k}) - i\tilde{b}_2(\mathbf{k})\right] \\ \tilde{v}_3(\mathbf{k}) &= \overline{\beta}\zeta_k^+\left[\tilde{u}_1(\mathbf{k}) + i\tilde{u}_2(\mathbf{k})\right] + \zeta_k^-\left[\tilde{b}_1(\mathbf{k}) + i\tilde{b}_2(\mathbf{k})\right] \\ \tilde{v}_4(\mathbf{k}) &= \overline{\beta}\zeta_k^+\left[\tilde{u}_1(\mathbf{k}) - i\tilde{u}_2(\mathbf{k})\right] - \zeta_k^-\left[\tilde{b}_1(\mathbf{k}) - i\tilde{b}_2(\mathbf{k})\right] \end{aligned}, \quad \begin{aligned} \zeta_k^\pm &\equiv \frac{1}{2}\sqrt{1 \pm \frac{\gamma}{k\eta_k}}, \\ \overline{\beta} &= \mathrm{sgn}(\beta). \end{aligned} \tag{2}$$

These equations give the transformed variables or 'eigenvariables' $\tilde{v}_i(\mathbf{k})$ for each mode and, implicitly, also give U_k and $\tilde{\mathsf{e}}_i(\mathbf{k})$. Note that the equations for $\tilde{v}_1(\mathbf{k})$ and $\tilde{v}_3(\mathbf{k})$ are decoupled from the equations for $\tilde{v}_2(\mathbf{k})$ and $\tilde{v}_4(\mathbf{k})$. The eigenanalysis results given here will help in the discussion of broken ergodicity in the next section.

4. Broken ergodicity

Each $\tilde{v}_i(\mathbf{k})$ is has its own $\lambda_k^{(i)}$, which are given in (1). The matrix $\mathsf{U}_k \in$ SU(4) so that $|\tilde{\mathbf{u}}(\mathbf{k})|^2 + |\tilde{\mathbf{b}}(\mathbf{k})|^2 = \Sigma_{i=1}^4 |\tilde{v}_i(\mathbf{k})|^2$, i.e., each side expresses the energy in mode **k**. However, we have seen that the largest-scale mode $\boldsymbol{\kappa}$ contains O(N) more energy than any of the other N–1

modes. If we assume that $H_M > 0$, it can be shown [8,11] that $\gamma < 0$. Then, looking at (1), we see that $\lambda_\kappa^{(4)} = \alpha - \frac{1}{2}\left(\eta_\kappa + |\gamma|/k\right)$ must be much smaller than any other $\lambda_\kappa^{(i)}$, i = 1,2,3, or any other $\lambda_k^{(i)}$, $k > \kappa$, i = 1,2,3,4. Analysis [8,11] reveals that the fraction of energy in statistical equilibrium that is expected to reside in $\tilde{v}_4(\boldsymbol{\kappa})$ is $\sim 1/\lambda_\kappa^{(4)} \sim 1$, while all other $\tilde{v}_i(\mathbf{k})$ are $\sim 1/\lambda_k^{(i)} \sim N^{-1}$; here, we have assumed $E = 1$, and that $H_M \neq 0$. Then, eigenvariable $\tilde{v}_4(\boldsymbol{\kappa})$ is O(1) as $N \to \infty$, while $\tilde{v}_i(\boldsymbol{\kappa}) \sim \varepsilon \approx 0$, for i = 1,2,3, and the equations for $\tilde{v}_1(\boldsymbol{\kappa})$ and $\tilde{v}_3(\boldsymbol{\kappa})$ in (2) will have left-sides that are O(ε); this is only achieved if $\tilde{u}_1(\boldsymbol{\kappa}) + i\tilde{u}_2(\boldsymbol{\kappa}) \approx \tilde{b}_1(\boldsymbol{\kappa}) + i\tilde{b}_2(\boldsymbol{\kappa}) \approx 0$, i.e., the negative helicity part of mode $\boldsymbol{\kappa}$ is zero. Thus, the positive helicity parts of the largest-scale mode $\boldsymbol{\kappa}$, $\tilde{u}_1(\boldsymbol{\kappa}) - i\tilde{u}_2(\boldsymbol{\kappa})$ and $\tilde{b}_1(\boldsymbol{\kappa}) - i\tilde{b}_2(\boldsymbol{\kappa})$, are maximal. Since $\tilde{u}_2(\boldsymbol{\kappa}) \approx i\tilde{u}_1(\boldsymbol{\kappa})$ and $\tilde{b}_2(\boldsymbol{\kappa}) \approx i\tilde{b}_1(\boldsymbol{\kappa})$, we have $\tilde{\mathbf{u}}(\boldsymbol{\kappa}) \approx i\boldsymbol{\kappa} \times \tilde{\mathbf{u}}(\boldsymbol{\kappa})$, $\tilde{\mathbf{b}}(\boldsymbol{\kappa}) \approx i\boldsymbol{\kappa} \times \tilde{\mathbf{b}}(\boldsymbol{\kappa})$ and $\tilde{\mathbf{u}}(\boldsymbol{\kappa}) \sim \tilde{\mathbf{b}}(\boldsymbol{\kappa})$, i.e., 'dynamic alignment' [10; pp. 78-79]. (These are Fourier case results [8], where $\kappa = 1$, but analogous results exist in the spherical geodynamo case [11], where $\kappa = 1.8638$.)

In terms of the ideal MHD equations [10], these results imply that $d \log|\tilde{v}_4(\boldsymbol{\kappa})|/dt \sim \varepsilon \approx 0$, while for all other eigenvariables, $d \log|\tilde{v}_i(\mathbf{k})|/dt \sim 1$. Although statistical theory [15] ostensibly predicted that all $\tilde{v}_i(\mathbf{k})$ have mean values of zero, this requires that all $\tilde{v}_i(\mathbf{k})$ have sufficiently strongly stochastic forcing. Here, we have seen that when ideal MHD turbulence is in statistical equilibrium, it has generally entered into a single helicity state at the largest scale and that this state is quantified by the eigenvariable $\tilde{v}_4(\boldsymbol{\kappa})$, which has far more energy than any other eigenvariable. This leads to a situation in which there is very little driving the eigenvariable $\tilde{v}_4(\boldsymbol{\kappa})$ to change its value and it becomes almost static, while all other other eigenvariables continue to be driven relatively strongly and appear to have zero mean values. Thus, in MHD turbulence, we have *broken ergodicity*, defined [16] as occurring when, 'In a system that is non-ergodic on physical timescales the phase point is effectively confined in one subregion or component of phase space.' Broken ergodicity manifests itself in MHD turbulence as a stationary structure at the largest scales of the volume containing a turbulent magnetofluid. It produces an effectively coherent structure out of seeming chaos. We will see a numerical example of this in the next section.

5. Numerical simulation

As an example of broken ergodicity, drawn from Fourier method MHD run 1a [6,8], consider fig. 1, showing $\mathrm{Re}\,\tilde{v}_i(\boldsymbol{\kappa})$ vs $\mathrm{Im}\,\tilde{v}_i(\boldsymbol{\kappa})$ from simulation time t = 0 to 200; + indicates the origin and • the initial point. Run 1a had $E = 1$, $H_C = 0.348$, $H_M = 0.092$, 64^3 grid points and 2×10^5 time steps ($\Delta t = 10^{-3}$). We have seen the same sort of behaviour in all of our ideal MHD runs ($0 \le |H_C| < E/2$; $0 < |H_M| < E$), as long as they have enough time steps and enough grid points. When dissipation is added for the same initial conditions, the $\tilde{v}_4(\boldsymbol{\kappa})$ begin to follow their ideal trajectories [6,8], but eventually turn back towards the origin as $E \to 0$. The majority of the energy in $\tilde{v}_4(\boldsymbol{\kappa})$ is magnetic; as $\kappa|H_M|/E \to 1$, energy becomes purely magnetic and concentrates at $\mathbf{k} = \boldsymbol{\kappa}$. However, if a mean field (i.e., constant in space and time) $\mathbf{B}_o$ is added to $\mathbf{b}$, $H_M \to 0$ with time, and the spectral peak at $\mathbf{k} = \boldsymbol{\kappa}$ disappears, while if the volume rotates with angular velocity $\boldsymbol{\Omega}_o$, the peak persists, but the energy in $\tilde{v}_4(\boldsymbol{\kappa})$ is essentially all magnetic. Furthermore, as $|\boldsymbol{\Omega}_o|$ increases, the dipole moment vector $\boldsymbol{\mu}$ begins to align with $\boldsymbol{\Omega}_o$, but the angle between them saturates relatively quickly as $|\boldsymbol{\Omega}_o|$ increases, at around 20° for simulations on a 32^3 grid [17] (an effect which remains to be explained theoretically).

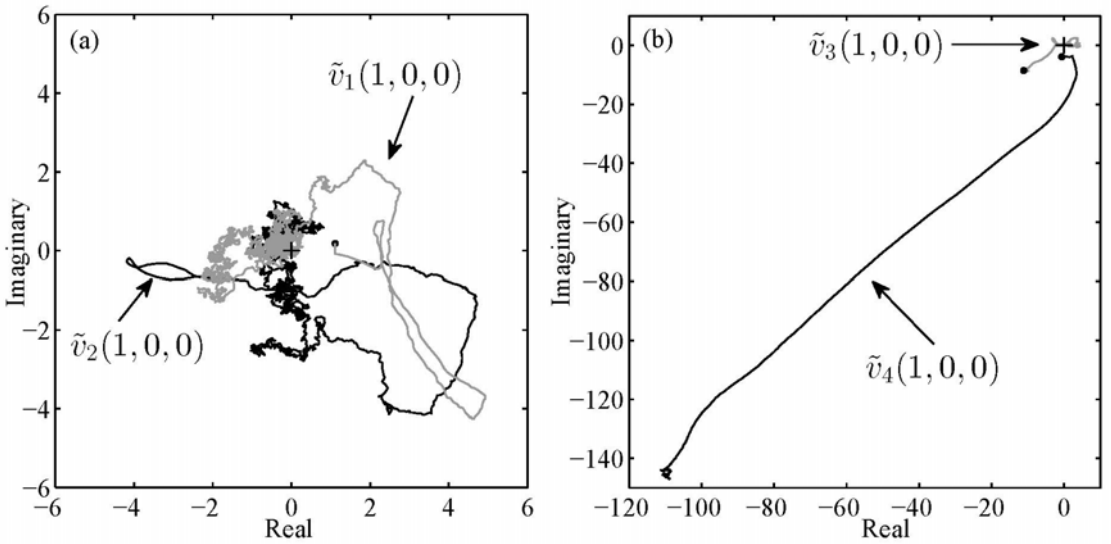

Figure 1: Evolution of (unnormalized) eigenvariables for $\boldsymbol{\kappa}$ = (1,0,0) from 64^3 run 1a [6].

6. Conclusion

Here, we have presented theoretical and numerical results concerning MHD turbulence and magnetic dynamos. The principle conclusion is that a statistical process involving broken ergodicity and magnetic helicity creates inherent dynamo action in MHD turbulence, causing the emergence of a large-scale, coherent magnetic field. This result may be relevant to understanding the oigin of planetary and stellar magnetic fields.

7. References

[1] Falgarone, E.; Passot, T.: Turbulence and Magnetic Fields in Astrophysics. Springer-Verlag, Berlin (2003).

[2] Jones, C.A.: Planetary Magnetic Fields and Fluid Dynamos. Annual Reviews of Fluid Mechanics 43 (2011) 583-614.

[3] Gailitis, A.; Lielausis, O.; Platacis, E.; Gerbeth, G.; Stefani, F.: Riga dynamo experiment and its theoretical background. Physics of Plasmas 11 (2004) 2838-2843.

[4] Shebalin, J.V.: Broken ergodicity and coherent structure in homogeneous turbulence. Physica D 37 (1989) 173-191.

[5] Shebalin, J.V.: Broken symmetry in ideal magnetohydrodynamic turbulence. Physics of Plasmas 1 (1994) 541-547.

[6] Shebalin, J.V.: Broken symmetries and magnetic dynamos. Physics of Plasmas 14 (2007) 102301.

[7] Shebalin, J.V.: Plasma relaxation and the turbulent dynamo. Physics of Plasmas 16 (2009) 072301.

[8] Shebalin, J.V.: Broken Ergodicity in Magnetohydrodynamic Turbulence. Geophysical and Astrophysical Fluid Dynamics 107 (2013) 411-466.

[9] Schubert, G. and Olson, P., Editors: Core Dynamics. Elsevier B.V., Amsterdam, NL (2009).

[10] Biskamp, D.: Magnetohydrodynamic Turbulence. Cambridge U.P., Cambridge, UK (2003) pp. 11-16.

[11] Shebalin, J.V.: Broken ergodicity, magnetic helicity and the MHD dynamo. Geophysical and Astrophysical Fluid Dynamics 107 (2013) 353-375.

[12] Glatzmaier, G.A. and Roberts, P.H.: A three-dimensional self-consistent computer simulation of a geomagnetic field reversal. Nature 377 (1995) 203-209.

[13] Khinchin, A.I.: Mathematical Foundations of Statistical Mechanics. Dover Books, NY (1949) 137-145.

[14] Kraichnan, R.H.: Helical turbulence and absolute equilibrium. Journal of Fluid Mechanics 59 (1973) 745-752.

[15] Frisch, U.; Pouquet, A.; Leorat, J.; Mazure, A.: Possibility of an inverse cascade of magnetic helicity in magnetohydrodynamic turbulence. Journal of Fluid Mechanics 68 (1975) 769-778.

[16] Palmer, R.G.: Broken ergodicity. Advances in Physics 31 (1982) 669-735.

[17] Shebalin, J. V.: Global invariants in ideal magnetohydrodynamic turbulence, Physics of Plasmas 20 (2013) 102305.